Supporting information

Simultaneous removal of Cr (VI) and TC over $BiO_{1-X}Br/CeVO_4$ S-scheme heterostructures: oxygen vacancies boosted charge separation and intermediates analysis

Haochun Zhang[a†], Ruyao Chen[a†], Xiufeng Zhou[d], Yuming Dong[c], Yigang Chen[b*], Haifeng Shi[a,d*]

[1] School of Science, Jiangnan University, Wuxi, 214122, P. R. China

[2] Department of General Surgery, The Affiliated Wuxi No. 2 People's Hospital of Nanjing Medical University, Wuxi, 214002, P. R. China

[3] School of Chemical & Material Engineering, Jiangnan University, Wuxi, 214122, P. R. China.

[4] National Laboratory of Solid State Microstructures, Nanjing University, Nanjing, 210093, P. R. China

Calculation

DFT calculations were performed using the Vienna Ab initio Simulation Package (VASP) code [1-3]. The structures of two-dimensional (2D) BOr and CeV bulk were optimized by the Perdew–Burke–Ernzerhof (PBE) of the generalized gradient approximation (GGA) [4-5]. A 520 eV cutoff energy was set after testing higher values to identify the accuracy. The 13×13×1 and 6×6×6 Gamma centered meshes were used to perform the Brillouin zone integration for 2D BOr and CeV bulk, respectively. An 18 Å vacuum space was added to eliminate the interaction between periodic cells. The electronic self-construct (SC) loop would be stopped if changes of total energy and eigenvalues between two steps were both smaller than 10^{-6} eV/atom for energy. In ionic

* E-mail addresses: hfshi@jiangnan.edu.cn (H.F. Shi), wuxichen2512@njmu.edu.cn (Y.G. Chen)

relaxation, all ionic positions, cell volume, and cell shape were optimized by the conjugate-gradient algorithm with a criterion that required the calculated forces less than 10^{-4} eV/Å.

The COMSOL Multiphysics theoretically modeled the electric field distribution calculations. The simulation domain comprises BOr with an air domain truncated. The diameter of the oxygen vacancy was set to 0.4 nm [6]. Maxwell's equations intended for the scattering of electromagnetic radiation near or in oxygen vacancies were solved in the company of the model. The interface used in this simulation was Electromagnetic Waves, Frequency Domain (emw) under the module Radio Frequency. The research was performed in 3D under the frequency domain.

[1] G. Kresse, J. Furthmuller, Efficient iterative schemes for ab initio total-energy calculations using a plane-wave basis set, Phys. Rev. B 54 (1996) 11169-11186.

[2] G. Kresse, J. Hafner, ABINITIO MOLECULAR-DYNAMICS FOR LIQUID-METALS, Phys. Rev. B 47 (1993) 558-561.

[3] G. Kresse, D. Joubert, From ultrasoft pseudopotentials to the projector augmented-wave method, Phys. Rev. B 59 (1999) 1758-1775.

[4] J.P. Perdew, K. Burke, M. Ernzerhof, Perdew, Burke, and Ernzerhof Reply, Phys. Rev. Lett. 80 (1998) 891-891.

[5] J.P. Perdew, K. Burke, M. Ernzerhof, Generalized gradient approximation made simple, Phys. Rev. Lett. 77 (1996) 3865-3868.

[6] X. C. Zhang, M. H. Guan, Q. R. Zhang, C. M. Zhang, R. Li, J. X. Liu, Y. W. Wang, C. M. Fan, First-principles study of single-atom Pt adsorption on BiOBr{001} surface with different atomic exposure terminations, Acta. Phys. Sin. 70 (2021) 087101.

Materials

The materials included potassium bromide (KBr), bismuth nitrate pentahydrate $(Bi(NO_3)_3 \cdot 5H_2O)$, polyvinyl pyrrolidone (PVP), diammonium cerium nitrate $(Ce(NH_4)_2(NO_3)_6)$, Ammonium vanadate (NH_4VO_3), ethylene glycol, and ethanol absoluter. All chemical reagents were of analytical grade and were used as received without further purification, and were purchased from Sinopharm Chemical Reagent Co., Ltd., China.
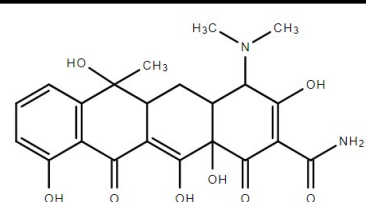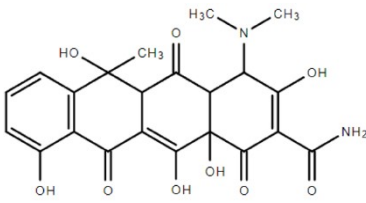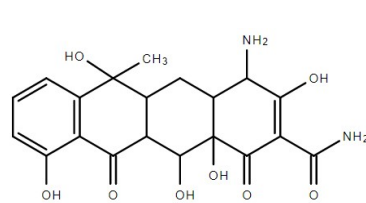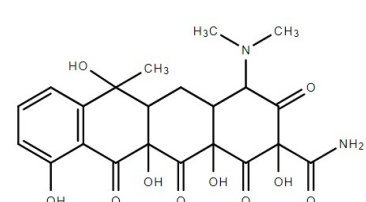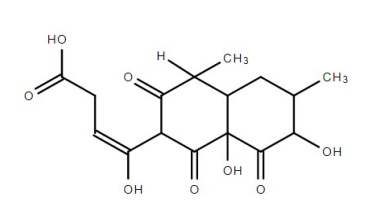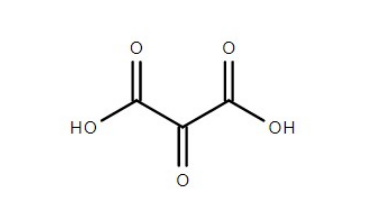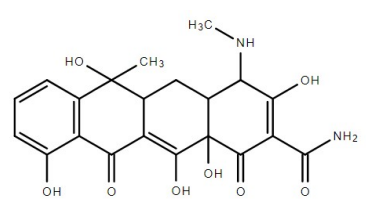
Materials characterization

The crystalline phases of as-prepared samples were analyzed by X-ray diffraction (XRD, DX2700 diffractometer, Haoyuan Instrument, P. R. China), which ran under Cu-Kα radiation with a scanning rate of 3°/min from 10° to 80°. UV-vis diffuse-reflection spectra (DRS) were collected with a UV-2600 spectrophotometer (Shimadzu, Japan), taking $BaSO_4$ as the reflectance standard. Transmission electron microscopy (TEM) of FEI Tecnai G2 F20 and scanning electron microscopy (SEM) were used to characterize the morphological characteristics of the CeV, BOr, BOr/CeV. Fourier transform infrared (FTIR) transmittance spectra of CeV, BOr, BOr/CeV nanocomposites were kept records with a Nicolet iS5 spectrometer (Thermo Fisher Scientific, USA) spectrometer. Electron paramagnetic resonance (EPR) analysis of the presence and concentration of OVs of the photocatalyst was performed by a spectrometer of Bruker ESP 500. X-ray photoelectron spectroscopy (XPS) measurements were performed using an ESCALAB 250xi (Thermo, USA) to estimate the chemical states. The photoluminescence (PL) spectra were evaluated using a fluorescence spectrophotometer FLSP920 (Edinburgh Instruments, UK) at an excitation wavelength of 325 nm.

Table S1 Comparison of performance of $BiO_{1-X}Br/CeVO_4$ with other photocatalysts for simultaneous photocatalytic TC removal and Cr (VI) reduction

Photocatalyst	Dosage (mg/L)	Pollutant(mg/L)		Degradation efficiency		Light source	Ref.
		TC	Cr(VI)	TC	Cr(VI)		
$BiO_{1-X}Br/CeVO_4$	0.5	20	5	83.12% (50min)	99.11% (25min)	300W XL, $\lambda \geq 420$ nm	**This work**
N-TiO$_2$/O-doped N vacancy g-C$_3$N$_4$	0.4	30	15	82.7% (60min)	100% (40min)	300W XL, $\lambda \geq 420$ nm	[1]
BCN-PA	0.25	30	10	89% (180min)	99% (180min)	300W XL, $\lambda \geq 420$ nm	[2]
AgI/BiVO$_4$	0.2	20	15	~90% (100min)	~70% (100 min)	500W XL, $\lambda \geq 420$ nm	[3]
Iron-modified rectorite/H$_2$O$_2$	0.4	100	10	97.5% (150min)	98.1% (150min)	500W LED $\lambda \geq 420$ nm	[4]
Co$_3$O$_4$/g-C$_3$N$_4$	0.4	15	15	92.6% (150min)	81.3% (150min)	500W XL, $\lambda \geq 420$ nm	[5]
BiVO$_4$-OV	1	20	10	81.22% (90min)	83.42% (90min)	300W XL, $\lambda \geq 420$ nm	[6]
TiO$_2$/BiOCl	1	30	15	97% (240min)	98% (180min)	300W XL, $\lambda \geq 400$ nm	[7]
MoS$_2$/B-rGO	0.4	20	20	85.3% (120min)	80.1% (120min)	300W XL, $\lambda \geq 420$ nm	[8]

[1] Y.X. Wang, L. Rao, P.F. Wang, Z.Y. Shi, L.X. Zhang, Photocatalytic activity of N-TiO$_2$/O-doped N vacancy g-C$_3$N$_4$ and the intermediates toxicity evaluation under tetracycline hydrochloride and Cr(VI) coexistence environment, Appl. Catal. B 262 (2020)118308.

[2] C.C. Yan, Y. Guo, P.F. Wang, L. Rao, X. Ji, Y. Guo, Improved photoremoval performance of boron carbon nitride–pyromellitic dianhydride composite toward tetracycline and Cr(VI) by itself to change the solution PH, New J. Chem. 44 (2020) 11105-11124.

[3] W. Zhao, J. Li, B.L. Dai, Z.P. Cheng, J.M. Xu, K.R. Ma, L.L. Zhang, N. Sheng, G.X. Mao, H.W. Wu, K.X. Wei, D. Y. C. Leung, Simultaneous removal of tetracycline and Cr (VI) by a novel three-dimensional AgI/BiVO$_4$ p-n junction photocatalyst and insight into the photocatalytic mechanism, Chem. Eng. J. 369 (2019) 716-725.

[4] S. Guo; W. Yang; L. You, J. Li, J. Chen; K. Zhou, Simultaneous reduction of Cr(VI) and degradation of tetracycline hydrochloride by a novel iron-modified rectorite composite through heterogeneous photo-Fenton processes. Chem. Eng. J. 393 (2020) 124758.

[5] W. Zhao, J. Li, T. She, S. Ma, Z. Cheng, G. Wang, P. Zhao, W. Wei, D. Xia, D. Y. C. Leung, Study on the photocatalysis mechanism of the Z-scheme cobalt oxide nanocubes/carbon nitride nanosheets heterojunction photocatalyst with high photocatalytic performances, J. Hazard. Mater. 402 (2021) 123839.

[6] S. Chen, B. Li, D.L. Huang, P. Xu, Y.S. Chen, L. Lei, Z.W. Wang, R. Deng, L. Du, G.F. Wang, Jointed Synchronous Photocatalytic Oxidation and Chromate Reduction Enabled by the Defect Distribution upon BiVO$_4$: Mechanism Insight and Toxicity Assessment, ACS Appl. Mater. Interfaces 13 (2021) 17586-17598.

[7] X. Hu, G. Zhang, C. Yin, C. Li, S. Zheng, Facile fabrication of heterogeneous TiO$_2$/BiOCl composite with superior visible-light-driven performance towards Cr (VI) and tetracycline, Mater. Res. Bull. 119 (2019) 110559.

[8] E. Vijayakumar, M. Govinda raj, B. Neppolian, S. Kumar Lakhera, A. John Bosco, Hierarchical layered nanostructure of MoS$_2$/boron doped reduced graphene oxide composites under visible light irradiation for effective antibiotic degradation and hexavalent chromium reduction, Mater. Lett. 296 (2021) 129891.
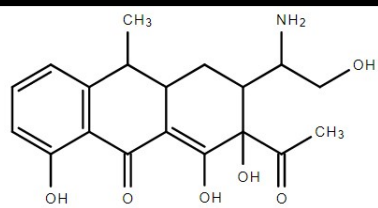
Table. S2. The structural information of the possible intermediates products.

Compounds	Formula	m/z	Proposed structure
TC	$C_{22}H_{24}N_2O_8$	445	
P1	$C_{22}H_{22}N_2O_9$	459	
P2	$C_{20}H_{20}N_2O_8$	415	
P3	$C_{22}H_{24}N_2O_{10}$	476	
P4	$C_{16}H_{20}O_8$	340	
P5	$C_3H_2O_5$	114	
P6	$C_{21}H_{22}N_2O_8$	432	

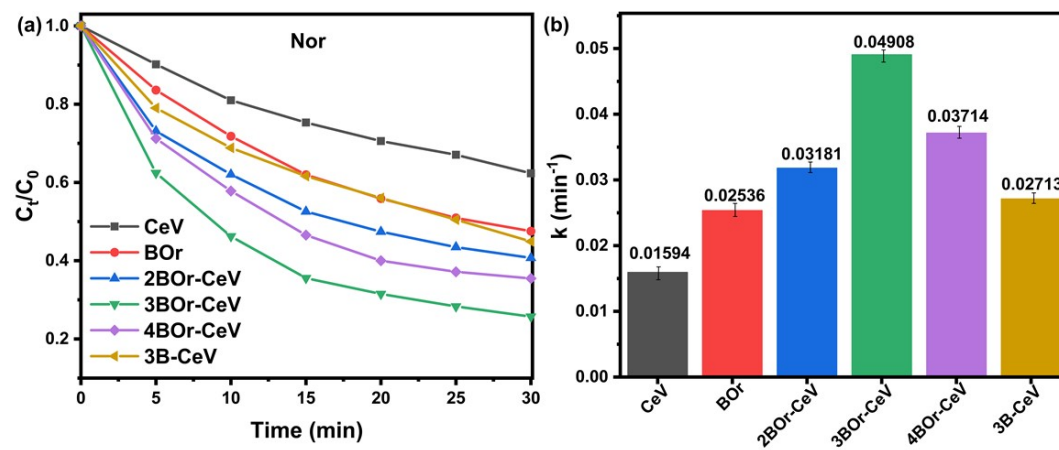|			
P7	$C_{19}H_{23}NO_6$	362	
P8	$C_{17}H_{18}O_6$	318	
P9	$C_{15}H_{14}O_5$	274	
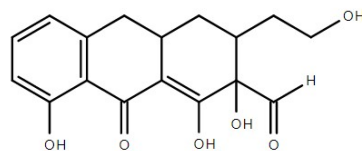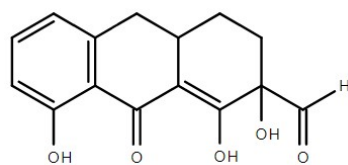
Fig. S1. (a) Photocatalytic degradation efficiencies of Nor, and (c) kinetic curves for the degradation of Nor using different photocatalysts.
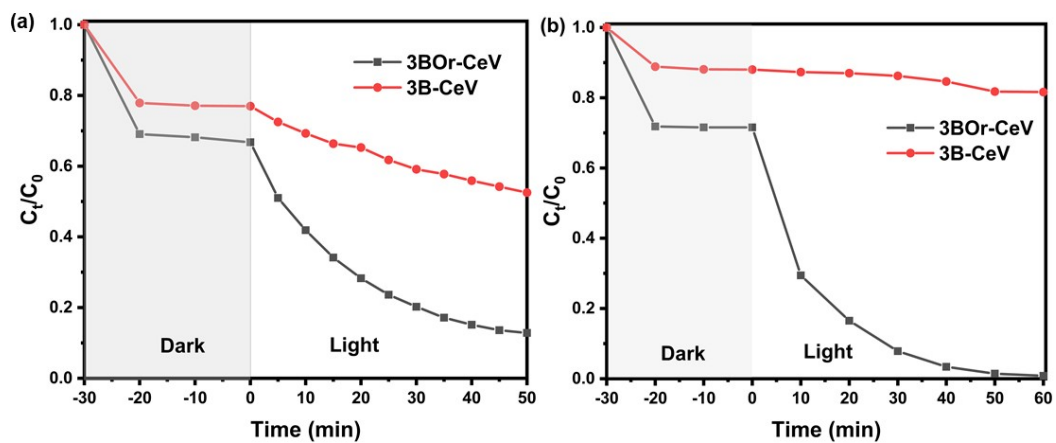
Fig. S2. The curves of (a) photocatalytic TC degradation and (b) photocatalytic Cr (VI) reduction for 3BOr-CeV and 3B-CeV with adsorption process under visible light.
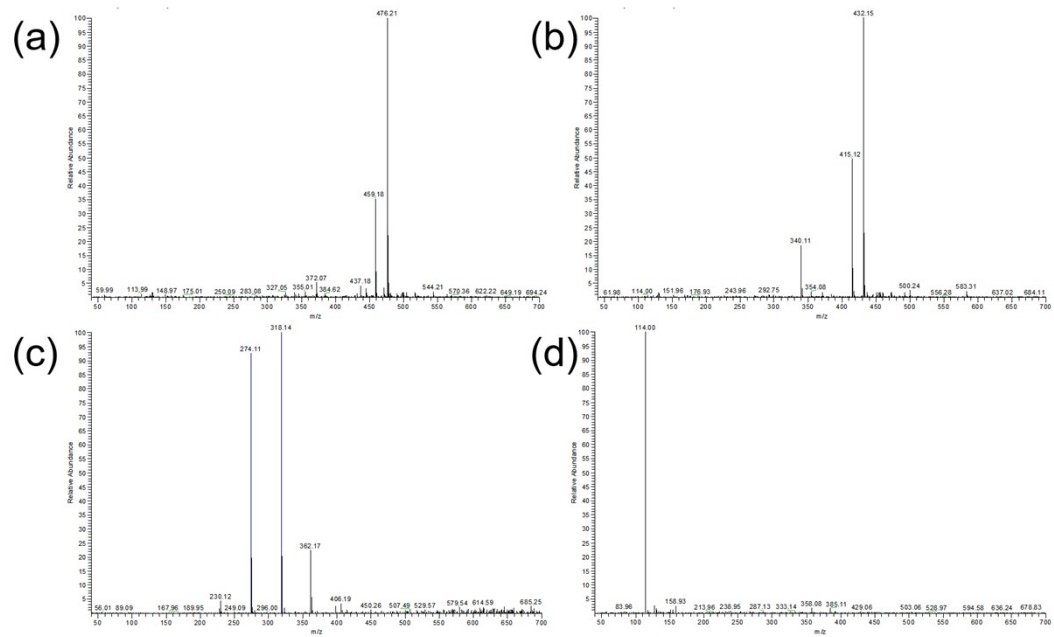
Fig. S3. Mass spectra for photocatalytic TC degradation with 3BOr-CeV at different moments: (a, b) 25 min; (c, d) 50 min
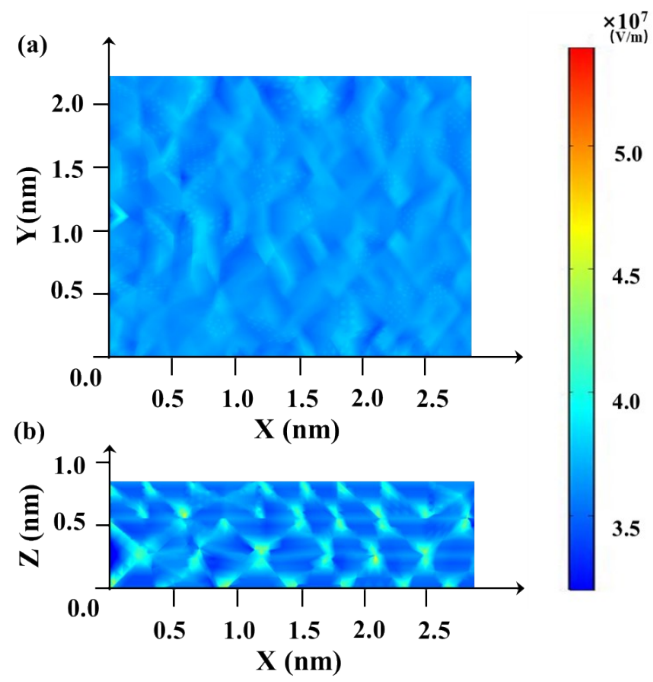
Fig. S4. Electric field distributions (a) horizontal cross-section, (b) vertical cross-section of BiOBr nanosheet using the COMSOL Multiphysics with visible light at a wavelength of 420 nm.